1. AGENCY USE ONLY (Leave blank)	2. REPORT DATE	3. REPORT TYPE AND DATES COVERED
	March 30 1994	Reprint

4. TITLE AND SUBTITLE
LARGE-SCALE CONVECTION PATTERNS OBSERVED BY DMSP

5. FUNDING NUMBERS
PE 61102F
PR 2311
TA G5
WU 04

6. AUTHOR(S)
Frederick J. Rich, Marc Hairston*

7. PERFORMING ORGANIZATION NAME(S) AND ADDRESS(ES)
Phillips Lab/GPSP
29 Randolph Road
Hanscom AFB, MA 01731-3010

8. PERFORMING ORGANIZATION REPORT NUMBER
PL-TR-94-2077

9. SPONSORING/MONITORING AGENCY NAME(S) AND ADDRESS(ES)

10. SPONSORING/MONITORING AGENCY REPORT NUMBER

11. SUPPLEMENTARY NOTES *Center for Space Science, University of Texas at Dallas, Richardson, Texas
Reprinted from Journal of Geophysical Research, Vol.99, No. A3, pages 3827-3844 March 1, 1994

12a. DISTRIBUTION/AVAILABILITY STATEMENT

Approved for public release; Distribution unlimited

13. ABSTRACT (Maximum 200 words)

Abstract. We present a comprehensive compilation of the average distribution of the electrostatic potential across the high-latitude ionosphere. The averages are compiled from potential along the satellite path calculated from thermal ion drift data from instrumentation on the Defense Meteorological Satellite Program (DMSP) flights 8 and 9 satellites. Data were collected from the DMSP F8 satellite during the period September 1987 to December 1990 and from the DMSP F9 satellite during the period March 1988 to December 1990. The potential distributions are separated by geomagnetic position, season, and orientation of the interplanetary magnetic field (IMF), and then averages of the distributions are calculated. The average potential distributions clearly show the displacement of polar cap convection contours to the dusk or dawn flanks under the influence of the IMF B_y component. The cross-cap potential decreases as IMF B_z changes from southward to northward. The average distributions indicate that the development of more than two convection cells for northward IMF is either uncommon or nonexistent. For IMF $B_z > 0$ and $B_z > |B_y|$, a distorted pattern is observed in the average potential distribution, not a four-cell pattern as some previous studies suggest it should be. For all orientations of the IMF, the convection reversal boundary at the poleward edge of the auroral zone is observed in the average distributions to be a rotational boundary. It is not a shear boundary as suggested by some previous investigations. On average, the Harang discontinuity (convection reversal in the auroral zone near midnight) is observed to exist weakly or not at all. When examining individual passes, a strong eastward flow is present sometimes in the region of the Harang discontinuity, especially on the poleward boundary, but not at all times as implied by the Heppner-Maynard model.

14. SUBJECT TERMS
DMSP, Ionosphere, Aurora, Ionosphere-Magnetosphere Coupling, Plasma convection

15. NUMBER OF PAGES
18

16. PRICE CODE

17. SECURITY CLASSIFICATION OF REPORT	18. SECURITY CLASSIFICATION OF THIS PAGE	19. SECURITY CLASSIFICATION OF ABSTRACT	20. LIMITATION OF ABSTRACT
UNCLASSIFIED	UNCLASSIFIED	UNCLASSIFIED	SAR

JOURNAL OF GEOPHYSICAL RESEARCH, VOL. 99, NO. A3, PAGES 3827-3844, MARCH 1, 1994

Large-scale convection patterns observed by DMSP

Frederick J. Rich

Phillips Laboratory, Geophysics Directorate, Hanscom AFB, Massachusetts

Marc Hairston

Center for Space Science, University of Texas at Dallas, Richardson, Texas

Abstract. We present a comprehensive compilation of the average distribution of the electrostatic potential across the high-latitude ionosphere. The averages are compiled from potential along the satellite path calculated from thermal ion drift data from instrumentation on the Defense Meteorological Satellite Program (DMSP) flights 8 and 9 satellites. Data were collected from the DMSP F8 satellite during the period September 1987 to December 1990 and from the DMSP F9 satellite during the period March 1988 to December 1990. The potential distributions are separated by geomagnetic position, season, and orientation of the interplanetary magnetic field (IMF), and then averages of the distributions are calculated. The average potential distributions clearly show the displacement of polar cap convection contours to the dusk or dawn flanks under the influence of the IMF B_y component. The cross-cap potential decreases as IMF B_z changes from southward to northward. The average distributions indicate that the development of more than two convection cells for northward IMF is either uncommon or nonexistent. For IMF $B_z > 0$ and $B_z > |B_y|$, a distorted pattern is observed in the average potential distribution, not a four-cell pattern as some previous studies suggest it should be. For all orientations of the IMF, the convection reversal boundary at the poleward edge of the auroral zone is observed in the average distributions to be a rotational boundary. It is not a shear boundary as suggested by some previous investigations. On average, the Harang discontinuity (convection reversal in the auroral zone near midnight) is observed to exist weakly or not at all. When examining individual passes, a strong eastward flow is present sometimes in the region of the Harang discontinuity, especially on the poleward boundary, but not at all times as implied by the Heppner-Maynard model.

Introduction

The electrostatic potential field that is imposed across the high-latitude ionosphere is a basic signature of the interaction of the solar wind and interplanetary magnetic field (IMF) with the Earth's magnetosphere and ionosphere. The electrostatic field causes a convective flow of ionospheric plasma. The basic two-cell convection pattern was first defined from ground-based observations by *Axford and Hines* [1961] and later confirmed with satellite observations such as those of *Heppner* [1972]. The convection electric field has been defined in greater, but somewhat conflicting, detail by later observations from ground-based observations [e.g., *Friis-Christensen et al.*, 1985; *Foster et al.*, 1986a, 1986b, 1989; and *Feldstein and Levitin*, 1986] and from satellite observations (see *Heppner and Maynard* [1987] and references therein). Much of our knowledge of the shape and size of the convection electric field comes from measurements which cover only a small portion of high-latitude ionosphere at any one time. Only a few studies, such as that done by *Kamide et al.* [1982], have been able to capture the full pattern at a moment in time.

The two-cell pattern of convection or equipotentials in the high-latitude regions has been clearly demonstrated in the observations under many circumstances. The magnitude of the potential field (or cross-cap potential drop) is affected by the direction and magnitude of the z components of the IMF. The dusk-to-dawn distribution of the electrostatic equipotential is affected by the direction of the y component of the IMF. In addition to the two-cell convection pattern, *Burke et al.* [1979] showed that when the z component of the IMF is northward, the convective pattern may have four cells. *Heppner and Maynard* [1987] have argued that there may not be four convection cells but two, very distorted cells for periods of northward ($B_z > 0$) IMF. Observations and interpretations of observations

Paper number 93JA03296.
0148-0227/94/93JA-03296$05.00

give modelers important clues in their effort to understand the solar wind-magnetosphere-ionosphere interaction. For example, *Reiff and Burch* [1985] have developed a model that implies that as the IMF B_z/B_y angle rotates from southward to northward, the convection pattern changes from two cells to three cells to four cells. *Toffeletto and Hill* [1989] have developed a model in which a portion of the polar ionosphere which connects to the IMF (i.e., open field lines) during periods of southward IMF may be closed field lines during periods of northward IMF.

To help determine the relationship between the IMF and the high latitude potential patterns, we have made use of a new and very extensive data set of ion drifts. We have constructed from many satellite passes a set of statistical convection patterns in order to put together a reasonably complete picture of the high-latitude region. Each pass covers only a limited region of the total pattern, but if the pattern is fundamentally the same under similar conditions, our survey is a very accurate description of the fundamental pattern.

In principle, the electric field observed in the topside, polar ionosphere is identical to the magnetospheric electric field since a classical resistance cannot be maintained along magnetic field lines in a collisionless plasma. *Weimer et al.* [1985] showed that this is only true for electric fields between 0 and a few hertz. Observations of electric fields parallel to the magnetic field lines at altitudes above 840 km have been reported by *Reiff et al.* [1988], *Burch et al.* [1990], and others. We will invoke the commonly made assumption that the parallel electric fields represent a minor change in the convection electric field between the magnetosphere and the polar ionosphere. Then, because only measurements of ion drifts due to quasi-stationary electric fields are used here, the convection patterns reported herein also represent the convection of plasma in the magnetosphere.

Instrumentation

All data presented in this report were obtained by the ion drift meter (IDM) which is part of the thermal plasma detector array (SSIES) carried on satellites of the Defense Meteorological Satellite Program (DMSP) starting with flight 8 of the block 5D series. The IDM measures the angle of arrival of ions. Since the thermal velocity of ions (especially O+ ions) is negligible with respect to spacecraft velocity, the arrival angle infers the component of the ion drift velocity perpendicular to the spacecraft's velocity.

The DMSP satellites are all intended to be in a polar (inclination = 98.8° ± 0.15°), circular (apogee/perigee = 848 ± 22 km), sun-synchronous orbit. The DMSP satellite series extend from the 1960s to the indefinite future. Since the 1970s, the DMSP satellites have carried instruments useful for investigation of the aurora and polar ionosphere. These include the low-light-level imager (OLS), the precipitating particle spectrometer (SSJ/3 and SSJ/4), the thermal plasma monitor (SSIES) and the flux-gate magnetometer (SSM). An ion drift meter, similar to ones flown on Atmospheric Explorer and Dynamics Explorer [*Heelis et al.*, 1981], is part of the SSIES array of thermal plasma sensors.

The ion drift meter measures angle of arrival of ions to a set of collector plates arranged behind a square, planar aperture mounted facing forward. The horizontal and vertical angles of arrival are converted into a horizontal and vertical ion drift from a known or assumed apparent ion drift along the track of the spacecraft. The apparent ion drift along the spacecraft track is the spacecraft speed (7.45 km s^{-1}) plus the component of ionospheric drift along the track. In this study, we have assumed the along-track component of the ionospheric drift to be zero. For most cases, this assumption introduces an error in the calculated horizontal and vertical drift of ±8% or less. The effective dynamic range of the IDM is ±2.7 km s^{-1} for ambient ion densities from 10^6 cm^{-3} to 5×10^3 cm^{-3}. When H+ or He+ ions represent more than 20% of the ambient plasma, the accuracy of the sensor is reduced and such data are discarded from our analysis. While the sensor has a resolution of 12 m s^{-1} for changes in the ion drift, it has an uncertainty which can be as large as 200 m s^{-1} in the absolute drift due to an uncontrolled zero level of the electronics. Since this zero level changes with a period of weeks, it is generally acceptable to calculate a zero level for each pass by assuming the measured ion drift (after accounting for corotation of the ionosphere) at midlatitudes is zero. The sensor in its standard mode makes six measurements of the horizontal flow per second and six measurements of the vertical flow per second. For the data analysis to support this study, a 4-s average and the variance each 4-s were calculated and used.

The first SSIES array was carried on the F8 spacecraft, and SSIES arrays have been carried on succeeding flights; see Table 1 for a summary of the present and anticipated data sets. In addition to the ion drift meter, the SSIES array contains an ion retarding potential analyzer (RPA), an ion total density trap (SM) and an electron Langmuir probe (EP). The RPA can determine the component of the ion flow parallel to the spacecraft velocity, the ion temperature, the total ion density and the ratio of O+ to H+ or He+. Unfortunately, the RPA data are not available for most F8 and all F9 data. The SM can determine the total ion density 24 times per second and can determine variations at rates up to 10 kHz. The EP can determine the electron temperature and potential of the instrument's ground with respect to the plasma. As shown in Figure 1, the array of ion sensors is mounted with the apertures flush to a conducting surface and the electron sensor is mounted on a short boom. The ion sensors' aperture plane prevents nonuniform electrostatic fields from altering the thermal ion trajectories as they approach the apertures. To keep the potential of the ion sensor apertures and the aperture plane very close to the plasma potential, a potential detector and feedback circuit (known as SENPOT) is used [*Zuccaro and Holt*, 1982]. For more details about the instrumentation, see *Greenspan et al.* [1986]. The SSIES-2 array listed in Table 1 contains the same sensors with improved electronics.

Table 1. DMSP Space Environment Instruments

Satellite	Launch Date	Ascending Node LT	Altitude km	End of Data	Space Environment Instrument
F8	June 87	0600	840	1994 (Est)	OLS, SSIES, SSJ/4
F9	Feb 88	1030	840	April 1992	OLS, SSIES, SSJ/4
F10	Nov 90	~2030	750-860	1994 (Est)	OLS, SSIES, SSJ/4
F11	Dec 91	1700	840	1995 (Est)	OLS, SSIES-2, SSJ/4
F12-F15	TBD	TBD	840 (Est)	TBD	OLS, SSIES-2, SSJ/4, SSM

OLS is the IR/visible imager that obtains white-light auroral images at night (very few images are available for 1989-1992). SSIES and SSIES-2 is the thermal plasma monitor which measures thermal ion drifts, ion density, and ion/electron temperatures. SSJ/4 is the precipitating particle spectrometer which measures the downward flux of 0.03-30 keV ions and electrons. which can be used to determine the auroral and polar cap boundaries, and the ionospheric conductivity. SSM is the vector magnetometer which measures field-aligned currents. Starting sometime in 1994, all DMSP data (including digital imaging data) will be available from National Oceanic and Atmospheric Administration / National Geophysical Data Center, Boulder, Colorado.

Data Analysis

The ion drift meter measures the flow of ions across the track of the satellite. Because the topside ionosphere is a collisionless plasma, the "frozen-in flux" approximation applies so that the ion drift perpendicular to the geomagnetic field (**B**) can be used to determine the convection electric field (**E**),

$$v_{\text{ion}} = \frac{\mathbf{E} \times \mathbf{B}}{\mathbf{B}^2} + v_{\parallel} \tag{1a}$$

or

$$\mathbf{E} = -v_{\text{ion}} \times \mathbf{B} \tag{1b}$$

where v_{ion} is the total ion drift velocity and $v_{\parallel}$ is the component of ion drift velocity parallel to the local magnetic field.

In our survey of the polar convection electric field we have chosen to survey the electrostatic potential instead of the components of ion drift from the drift me-

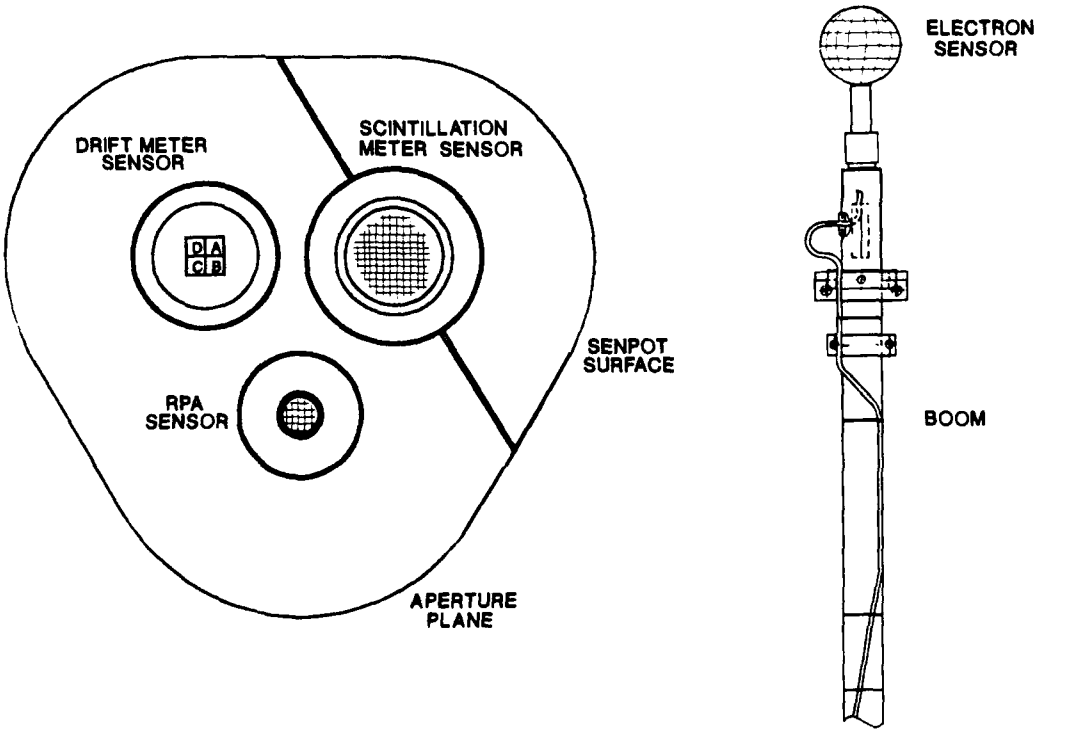

Figure 1. View of the ion and electron sensors. The three ion sensors are mounted flush to a plane which is electrostatically uniform at a potential approximately equal to the plasma potential and facing forward. The array of ion sensors and aperture plane are mounted on the spacecraft's forward surface. The electron sensor is mounted at the end of a 28 inch (71 cm) boom projecting radially upward with respect to the Earth.

compensate for the fact that the auroral oval expands with increasing activity level. The activity level is determined from the location of the equatorward edge of the auroral oval as determined from the simultaneous observations of precipitating 0.03 - 30 keV electrons [*Gussenhoven et al.* 1983; and *Madden and Gussenhoven* 1990]. The magnetic coordinates of the satellite track are adjusted so that the observed oval matches the oval observed for conditions of $Kp = 3+$. This tends to reduce spreading of the average pattern due to fluctuations in the size of the auroral zone. The calculation is done as follows

$$Kp' = (67.25° - \mathrm{MB})/1.697° \tag{4a}$$

where $Kp'$is the effective Kp index determined from the DMSP precipitating electron data and MB is the equatorward boundary of the precipitating electrons projected to the midnight meridian.

The auroral oval can be described as a circle with

$$\text{radius} = 21.2° + 1.58°Kp' \tag{4b}$$

centered at 3 hrs magnetic local time and $90° - (2.4° + 0.36°Kp')$. The coordinates of the observations are transformed to the circle for Kp' of 3.33.

This method for adjusting the size of the high-latitude region may not be ideal but it has proven to be better than making no adjustment at all.

3. The measured potential at each 4-s interval along the pass is tagged with the value of the interplanetary magnetic field (IMF) measured on the IMP 8 satellite in the solar wind. (The IMP 8 IMF data were provided as a vector each 15 s. We translated the observed time to a time equivalent to the passage of the solar wind passing $X_{SE} = 0$ using a "typical" solar wind speed of 450 km s^{-1}. We then built 5-min averages to filter out IMF fluctuation which do not affect the global magnetospheric potential.) Each measured potential is matched with the average of the IMF for the period 0 to 10 min before the equivalent time of the measurement. This delay time was chosen because the dayside of the convection pattern seems to react to changes in the IMF at the magnetopause with a 5- to 10-min delay, while the nightside of the pattern tends to react with timescales up to 30 min [*Lockwood et al.*, 1990; *Lockwood and Cowley*, 1991 and references therein]. Also, there is evidence that the nightside of the convection pattern filters out higher-frequency fluctuations of the IMF better than the dayside due to the "fly wheel" effect of energy stored in the magnetotail. Thus we have chosen a time constant to best fit the dayside of the pattern.

4. The measured potentials for a pass are sorted into spatial bins of one-half hour of magnetic local time by 1° of corrected geomagnetic latitude for latitudes from 50° to 87°. From 87° to 89° the bin size is 2 hours by 1°. All measurements poleward of 89° go into one bin. There may be several 4-s samples of the potential from one satellite pass in a given bin; if there are, they are averaged together to make one item to be entered into the bin for a single satellite pass.

While almost all magnetic local times above 50° are covered, it should be kept in mind that only four geographic local times are covered by the two satellites. The offset of the magnetic pole from the geographic pole allows a broad range of magnetic local times to be covered. This introduces the possibility that variations in the auroral structure due to universal time are represented instead as variations in magnetic local time. No effort has been made in this study to find and remove any possible UT effect.

Each spatial bin with data is tagged with the IMF value tagged to the first value in the bin. The average potential in a spatial bin is added to a sum of potentials for previously processed passes in a spatial-IMF set of bins, and an index for the number of entries in the spatial-IMF bin is incremented. The IMF levels for the spatial-IMF bins consist of eight different ranges of the IMF B_y/B_z angle ($0°, 45°, 90°, \ldots, 315° \pm 22.5°$) and three different levels of the magnitude of B (0 - 5, 5 - 11, and > 11 nT). If no IMF data are available, the measured potentials are not used. Figure 2 shows the distribution of the magnitude of the IMF and the B_y and B_z for the period January 1, 1988 to December 31, 1990. The bimodal distribution of the IMF B_y component reflects the tendency for the IMF to make an angle of $-45°$ or $+135°$ with respect to the Earth-Sun line. If IMF data is available and the satellite is in the southern hemisphere, the sign of B_y is reversed to account for the hemispheric asymmetry caused by the B_y component.

The potentials are separated according to the value of the IMF in order to account for the transfer rate of energy from the solar wind to the magnetosphere. Previous studies (*Reiff and Luhmann* [1986], *Ahn et al.* [1992], and others) have shown that there is a correlation between the value of the IMF and geomagnetic activity. These same studies have shown that a combination of solar wind parameters and the IMF give a higher correlation. Unfortunately, no solar wind data is available for the period of the DMSP ion drift data. To determine the relationship between geomagnetic activity and the measured potentials, the DMSP data were also separated using the Kp index, but it was found that the value of the IMF did a better job of organizing the data.

The number of passes available during the equinox periods of this study and the number of passes used after discarding passes for the reasons given above is shown in Figure 3. It is obvious that the limit availability of IMF data had a strong effect, but there are more than enough passes when IMF is available to provide meaningful results.

5. When sorting the "good," observed potentials, the F8 and F9 satellite measurements are combined. Since the electrostatic potential is a scalar, measurements from different satellite tracks can be combined readily. To be sure that this was really true, we plotted F8 and F9 data separately and compared the results in the overlay region.

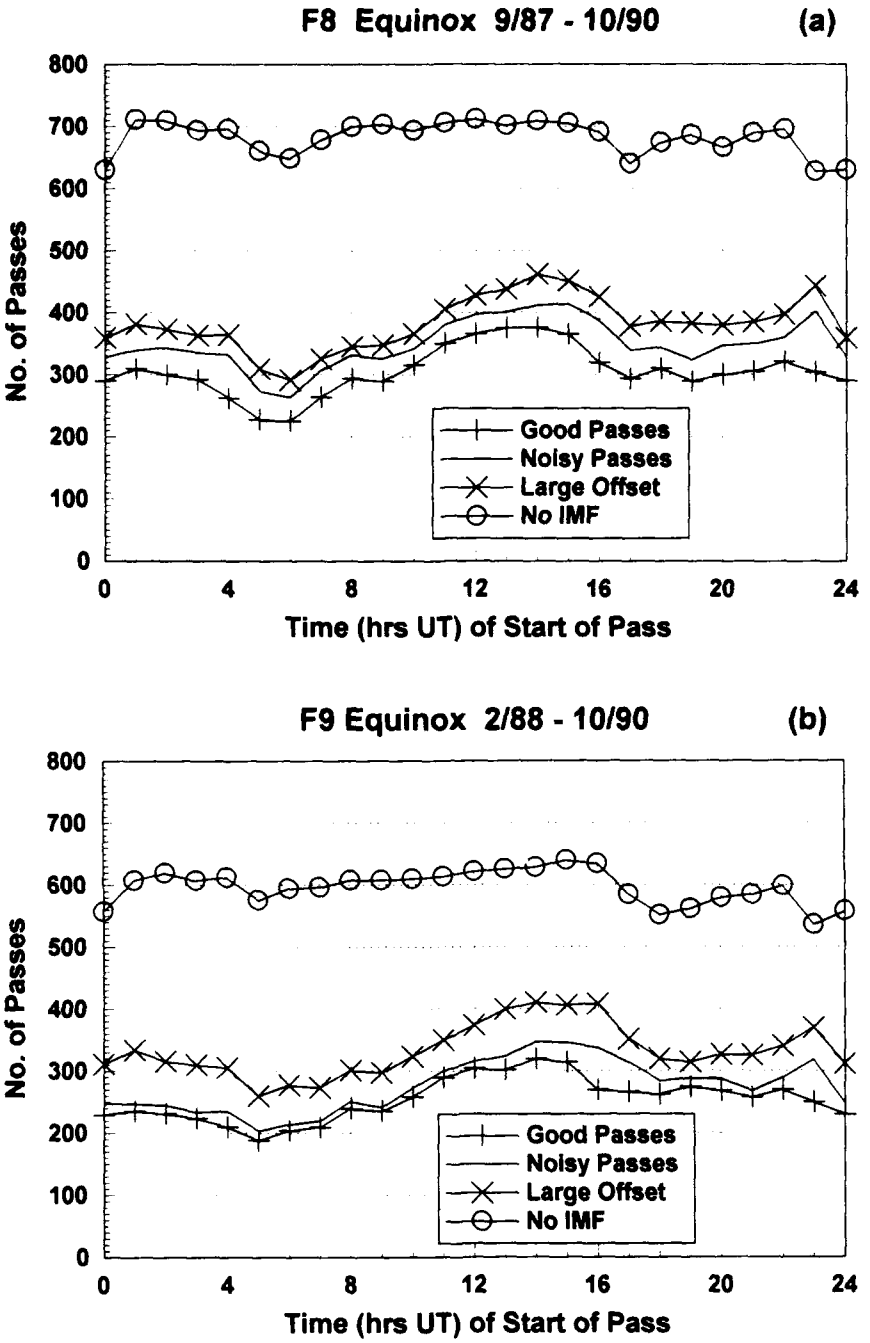

Figure 3. Number of passes DMSP passes as a function of time of day at the start of a pass for the equinox periods used in this study. The top line indicates the total number of passes available. The area between the top line and the next line represents the the number of passes unusable due to the lack of IMF data. The area between the second and third lines down represents and the shaded area indicates the number of passes unusable due to large potential offsets. The area between the third and fourth lines down represent the number of passes unusable because of poor signal to noise ratio ("Noisy"). The area below the bottom line represent the number of passes used ("Good"). The number of passes are shown for (a) the F8 satellite and (b) the F9 satellite.

8. Contour plots are created from the averaged, binned data to allow easy comparison with previous potential models derived from theory or analysis of other data. Since there are statistical fluctuations in the data, a smoothing of the data is required to avoid meaningless small-scale structures in the contours. Because typical analytical smoothing algorithms also drive the maximum and minimum values toward the average value,

the smoothing was done manually, and because the contours were created manually, a digital representation of the contours does not exist.

Results

In Figures 4 through 8, a significant portion of the results obtained are shown as contour plots of the equipotentials in geomagnetic coordinates which have been adjusted to an auroral oval size appropriate for $Kp = 3$ and for the northern high-latitude region. For observations in the southern region, the sign of the IMF B_y component is reversed. In all of these cases, the contour plots represent an "average" pattern. Table 2 gives the value and location of the maximum and minimum potential for all of the patterns.

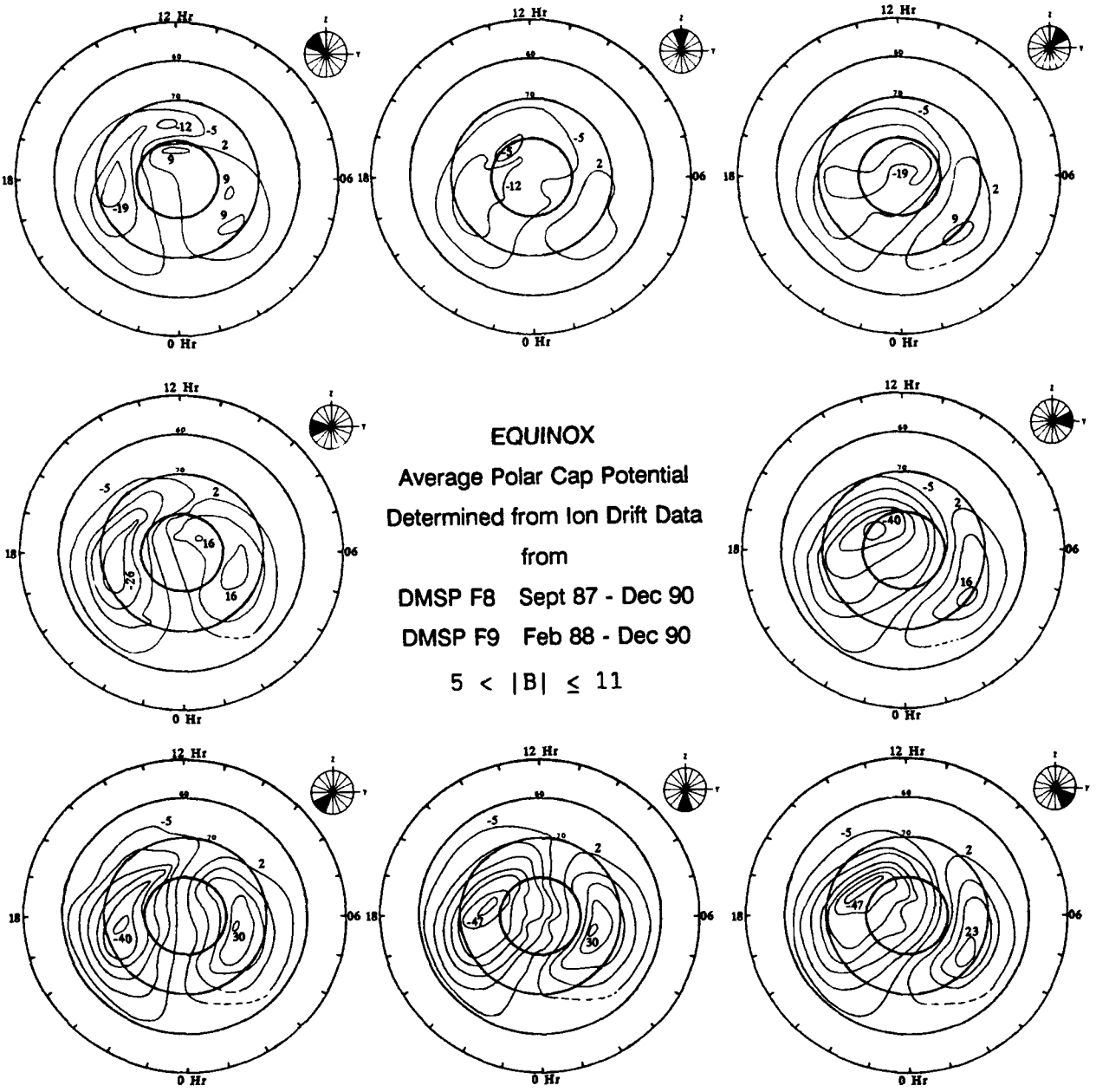

Figure 4. Contours drawn through the average potentials calculated ion drift meter data obtained from DMSP F8 and F9 during the period September 1987 to December 90. Equinox contours shown here were made by selecting data in both hemisphere during the months of February to April and August to October. The data were further selected for periods when IMF were data available, for 5 nT $<| B |\leq$ 11 nT and for eight ranges of the IMF B_y/B_z angle. Dashed contours indicate regions where no data were available. While data were obtained from both hemispheres, the contours are displayed as seen in the northern hemisphere. Each contour represents a change of 7 kV.

Table 2. Statistical Maximum and Minimum Potentials

IMF |B|	Season	Theta	Maximum Potential	MLT hours	Magnetic Latitude	Minimum Potential	MLT hours	Magnetic Latitude
0 – 5	Equinox	$B_y \gg \|B_z\| > 0$	11	2	66	−36	14.5	81
0 – 5	Equinox	$B_y > 0, B_z > 0$	12	2.5	69	−30	15	77
0 – 5	Equinox	$B_z \gg \|B_y\| > 0$	10	3.5	70	−28	19	76
0 – 5	Equinox	$B_y < 0, B_z > 0$	12	4	75	−23	17	73
0 – 5	Equinox	$\|B_y\| \gg \|B_z\|, B_y < 0$	15	7.5	80	−39	16	76
0 – 5	Equinox	$B_y < 0, B_z < 0$	18	3	71	−36	17	76
0 – 5	Equinox	$\|B_z\| \gg \|B_y\|, B_z < 0$	22	3.5	71	−41	17	77
0 – 5	Equinox	$B_y > 0, B_z < 0$	29	13.5	61	−39	16.5	75
5 – 11	Equinox	$B_y \gg \|B_z\| > 0$	18	2.5	70	−43	16	82
5 – 11	Equinox	$B_y > 0, B_z > 0$	10	2.5	69	−25	10.5	84
5 – 11	Equinox	$B_z \gg \|B_y\| > 0$	6	3	69	−19	18.5	74
5 – 11	Equinox	$B_y < 0, B_z > 0$	13	10.5	82	−23	18.5	75
5 – 11	Equinox	$\|B_y\| \gg \|B_z\|, B_y < 0$	19	4.5	75	−33	17.5	73
5 – 11	Equinox	$B_y < 0, B_z < 0$	31	5	77	−44	18.5	73
5 – 11	Equinox	$\|B_z\| \gg \|B_y\|, B_z < 0$	31	5	76	−51	15.5	80
5 – 11	Equinox	$B_y > 0, B_z < 0$	26	3	72	−51	16.5	77
>11	Equinox	$B_y \gg \|B_z\| > 0$	25	3	70	−60	13.5	80
>11	Equinox	$B_y > 0, B_z > 0$	18	3	69	−50	15.5	84
>11	Equinox	$B_z \gg \|B_y\| > 0$	7	2.5	67	−22	19.5	75
>11	Equinox	$B_y < 0, B_z > 0$	25	7	82	−33	17	72
>11	Equinox	$\|B_y\| \gg \|B_z\|, B_y < 0$	40	10	79	−44	17.5	74
>11	Equinox	$B_y < 0, B_z < 0$	44	5	76	−61	16	75
>11	Equinox	$\|B_z\| \gg \|B_y\|, B_z < 0$	44	6.5	75	−71	17	71
>11	Equinox	$B_y > 0, B_z < 0$	34	5	75	−78	15.5	76
0 – 5	Summer	$B_y \gg \|B_z\| > 0$	10	2.5	67	−32	14.5	81
0 – 5	Summer	$B_y > 0, B_z > 0$	14	6.5	73	−26	18	79
0 – 5	Summer	$B_z \gg \|B_y\| > 0$	10	5	77	−22	19	76
0 – 5	Summer	$B_y < 0, B_z > 0$	12	4	75	−27	16	75
0 – 5	Summer	$\|B_y\| \gg \|B_z\|, B_y < 0$	14	4	77	−24	16	77
0 – 5	Summer	$B_y < 0, B_z < 0$	18	7	76	−43	17	73
0 – 5	Summer	$\|B_z\| \gg \|B_y\|, B_z < 0$	20	4	69	−42	17	80
0 – 5	Summer	$B_y > 0, B_z < 0$	14	4	72	−43	15.5	75
5 – 11	Summer	$B_y \gg \|B_z\| > 0$	6	3	69	−37	14	83
5 – 11	Summer	$B_y > 0, B_z > 0$	5	3	69	−32	12	82
5 – 11	Summer	$B_z \gg \|B_y\| > 0$	5	2.5	67	−22	15	77
5 – 11	Summer	$B_y < 0, B_z > 0$	14	9.5	82	−25	17	75
5 – 11	Summer	$\|B_y\| \gg \|B_z\|, B_y < 0$	23	9.5	84	−28	17.5	72
5 – 11	Summer	$B_y < 0, B_z < 0$	26	6	75	−45	16.5	74
5 – 11	Summer	$\|B_z\| \gg \|B_y\|, B_z < 0$	31	6.5	73	−50	17	75
5 – 11	Summer	$B_y > 0, B_z < 0$	15	5.5	71	−52	16	82
>11	Summer	$B_y \gg \|B_z\| > 0$	16	3.5	67	−67	15.5	81
>11	Summer	$B_y > 0, B_z > 0$	12	9.5	72	−65	17.5	83
>11	Summer	$B_z \gg \|B_y\| > 0$	16	18	87	−32	10	78
>11	Summer	$B_y < 0, B_z > 0$	31	4.5	83	−23	18	71
>11	Summer	$\|B_y\| \gg \|B_z\|, B_y < 0$	42	9.5	82	−38	17.5	76
>11	Summer	$B_y < 0, B_z < 0$	49	7.5	75	−58	15	73
>11	Summer	$\|B_z\| \gg \|B_y\|, B_z < 0$	38	5	72	−68	17	72
>11	Summer	$B_y > 0, B_z < 0$	22	6	72	−68	15	76
0 – 5	Winter	$B_y \gg \|B_z\| > 0$	15	2.5	67	−36	14.5	83
0 – 5	Winter	$B_y > 0, B_z > 0$	14	3.5	69	−25	16.5	76
0 – 5	Winter	$B_z \gg \|B_y\| > 0$	31	13.5	63	−24	20.5	68
0 – 5	Winter	$B_y < 0, B_z > 0$	16	2.5	76	−28	18.5	77
0 – 5	Winter	$\|B_y\| \gg \|B_z\|, B_y < 0$	12	3	73	−28	20	71
0 – 5	Winter	$B_y < 0, B_z < 0$	34	5.5	75	−33	18	71
0 – 5	Winter	$\|B_z\| \gg \|B_y\|, B_z < 0$	25	6	75	−40	19.5	74
0 – 5	Winter	$B_y > 0, B_z < 0$	21	4.5	74	−39	16	77
5 – 11	Winter	$B_y \gg \|B_z\| > 0$	20	3	71	−37	16.5	80
5 – 11	Winter	$B_y > 0, B_z > 0$	27	16	69	−30	15.5	78
5 – 11	Winter	$B_z \gg \|B_y\| > 0$	18	16	65	−23	17.5	77
5 – 11	Winter	$B_y < 0, B_z > 0$	29	11.5	81	−20	21	71
5 – 11	Winter	$\|B_y\| \gg \|B_z\|, B_y < 0$	23	13	84	−35	15	58
5 – 11	Winter	$B_y < 0, B_z < 0$	31	5	77	−42	20	71
5 – 11	Winter	$\|B_z\| \gg \|B_y\|, B_z < 0$	29	6	75	−48	15	75
5 – 11	Winter	$B_y > 0, B_z < 0$	29	5.5	77	−51	17	74

Table 2. (continued)

IMF |B|	Season	Theta	Maximum Potential	MLT hours	Magnetic Latitude	Minimum Potential	MLT hours	Magnetic Latitude
>11	Winter	$B_y \gg \|B_z\| > 0$	29	4	71	−85	22.5	76
>11	Winter	$B_y > 0, B_z > 0$	18	2.5	69	−34	10	80
>11	Winter	$B_z \gg \|B_y\| > 0$	24	14	69	−27	20.5	69
>11	Winter	$B_y < 0, B_z > 0$	16	1.5	76	−37	16	72
>11	Winter	$\|B_y\| \gg \|B_z\|, B_y < 0$	44	14	85	−43	20	70
>11	Winter	$B_y < 0, B_z < 0$	47	7.5	81	−52	19	72
>11	Winter	$\|B_z\| \gg \|B_y\|, B_z < 0$	54	8	80	−71	17	71
>11	Winter	$B_y > 0, B_z < 0$	57	5.5	77	−70	16	76

The average patterns developed in this study tend to be missing features related to the dynamics of the ionosphere-magnetosphere connection that other investigators have suggested as a function of the rate of change in the IMF components or as a function of the phase of a substorm. While we have not specifically selected periods when the IMF direction and magnitude is steady, the "average" patterns should be approximately the same as the patterns for a steady state of the IMF. The IMF, on a scale of tens of minutes, is more often steady than rapidly fluctuating. *Rostoker et al.* [1988] and *Lockwood* [1991] have shown that the median time for the IMF B_z polarity to be maintained is approximately 30 min. The statistical weighting of these steady periods tend to outweigh observations obtained when the IMF is rapidly changing.

In Figures 4 through 7, the contour plots for one season (equinox, summer or winter), for one level of range of the magnitude of the IMF and for all eight ranges of the IMF B_y / B_z angles are shown. By comparing Figures 4, 5, and 6, one can see the change in the convection pattern with the change in season. By comparing Figure 4 and 7, one can see the change in the convection pattern with changes in the magnitude of the IMF.

Several features are common to most orientations and magnitudes of the IMF. The convection reversal line is the loci of latitudes in the auroral zone on morning and evening sectors at or near the polar cap boundary where sunward convection changes to antisunward convection. The convection reversal line obtained from our statistical model is a rotational discontinuity (potential contours and ion bulk flow cross the line or boundary). It is not a shear discontinuity (potential contours parallel and the electric field perpendicular to the line or boundary). The "throat" near the dayside cusp, first identified by *Heelis et al.* [1976], is a region of a few degrees in latitude near the noon meridian, where the ion flow is very rapid ($\gg$1 km s^{-1}). In our statistical model there is no "throat" near dayside cusp. If the "throat" is a feature of the quasi-steady state convection pattern but is a dynamic feature in location and magnitude, then the variance of the potential (which was calculated but is not shown) near the ionospheric projection of the dayside cusp should be higher than for other regions, but it is not. On the other hand, the variance of the electric field in that region is very large for scale sizes from 2° in latitude to the smallest scale that can be observed (which is 2 km for the DMSP drift meter). It is not unusual to observe ion drifts of 2 km s^{-1} in the dayside cusp region over a distance of only a few tens of kilometers with adjacent regions of rapid ion convection in the opposite direction. The integration of the electric field through the dayside cusp region yields small-scale changes to the potential but does not yield a significant ($\gg$10 kV) potential drop. For $|B_y| \gg 0$ and $B_z < 0$, the flow near dayside cusp is nearly E-W; this flow is similar to the pattern described by *Heppner and Maynard* [1987].

The variance of the potentials shown is generally in the range of 5 to 15 kV in the auroral zone and polar cap near midnight and rises to 10 to 20 kV in the dayside half of the pattern for the |B| range of 5 to 11 nT. There is only a slight increase in these variances with increasing |B|. The highest variances are 20 to 30 kV near the minimum potential for $|B_y| \gg 0$ and $B_z < 0$. Much of the variance can be attributed to the fact that we did not try to eliminate periods of rapidly changing geophysical conditions. Such a selection would reduce the variance somewhat but would have increased the statistical uncertainty for many sections of the patterns which are supported by a limited number of passes. One should compare our results with the results of other studies [e.g. *Lu et al.* 1993 and *Cumnock et al.* 1992] in which data were selected for periods of slowly varying geophysical conditions.

In Figure 8 the contours for IMF $B_z > 0$ and IMF $B_y \sim 0$ are shown with a smaller increment in the contour levels than in the other figures. This allows one to see the distorted convection pattern we have found. The convection patterns for northward IMF are clearly not the multicell convection pattern suggested by *Burke et al.* [1979] nor are they exactly the same as the distorted two-cell convection pattern of *Heppner and Maynard* [1987]. In fact, the results could be described as a three- or four-cell pattern, but the extra cell(s) does(do) not seem to be independent convection cell(s). Rather, the extra cell(s) is(are) superimposed on the afternoon cell of the two-cell pattern. We cannot make an unambiguous statement about the extra cell(s) from this study because the individual passes have a range of characteristics from no extra convection cell to very strong convection in the region of the extra cell. Studies with multiple, simultaneous satellite and ground-based data sets, such as being done by *Lu et al.* [1993], will be

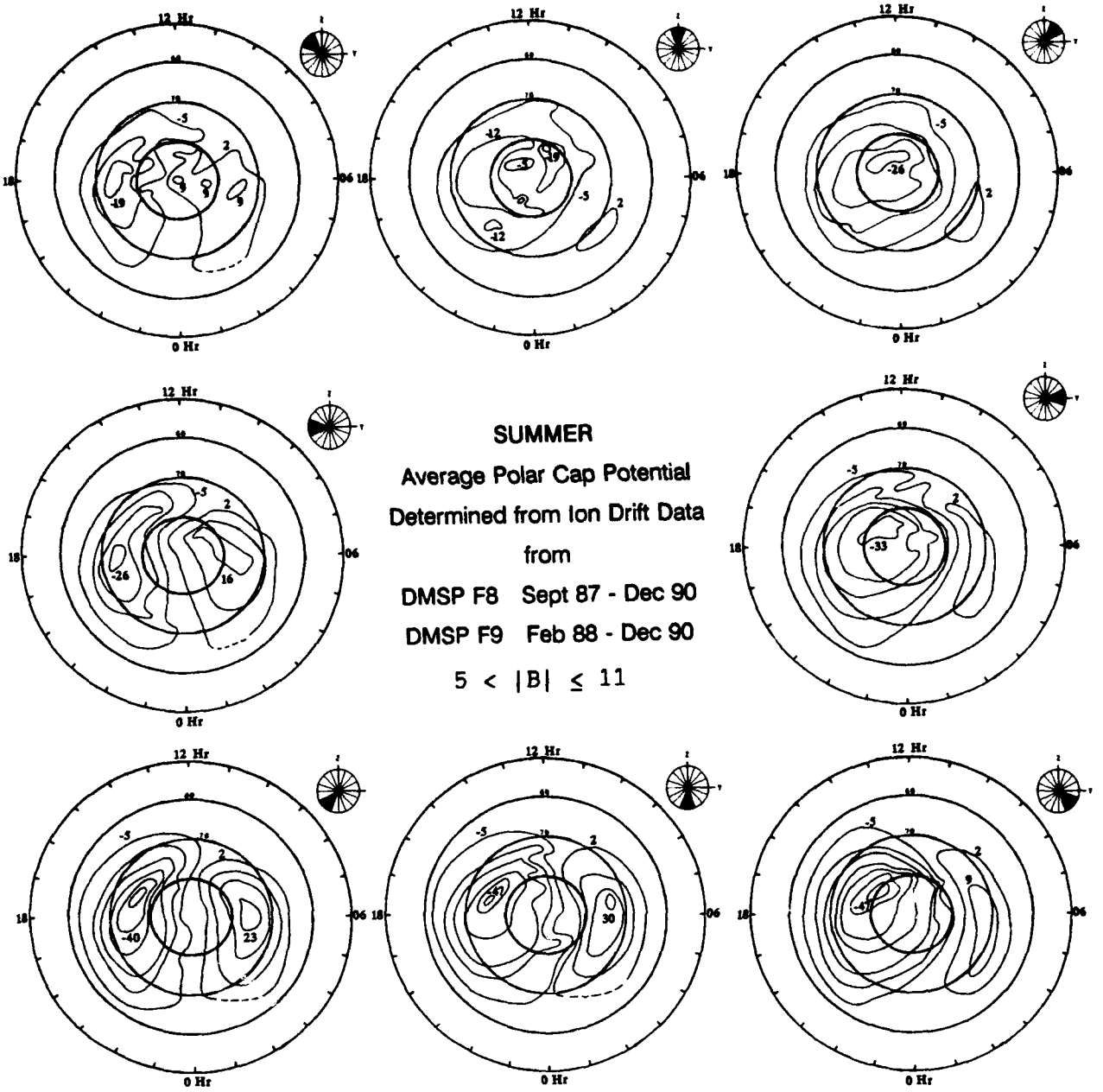

Figure 5. Contours drawn through the average potentials from DMSP F8 and F9 ion driftmeter data obtained during Summer Solstice periods and for times when IMF data are available and $5 < | B | \leq 11$ nT. The data are separated into eight groups based on the IMF B_y/B_z angle. Format is identical to that of Figure 4. Summer Solstice is defined to be May to July in the northern hemisphere and November to January in the southern hemisphere.

required to answer this question. In Figure 8 it is clear that the morning cell shrinks in size and tends to rotate toward midnight. This is similar to results obtained by *Knipp et al.* [1991] and *Lu et al.* [1993].

Discussion and Conclusions

Several features about the average convection patterns can easily be seen from an inspection of the contour plots created from our survey data:

1. The high-latitude potential distribution is a two-cell convection pattern and the two-cell pattern is present for all conditions of season and IMF. For IMF $B_z > 0$ and $|B_y| \geq B_z$, the two-cell convection pattern is distorted from the pattern maintained by southward IMF, but the convection patterns with three or four individual cells as previously suggested are not present. For IMF $B_z > 0$ and $|B_y| \ll B_z$, the pattern is a distorted two-cell pattern with evidence for two extra cell imbedded in the afternoon cell. The pattern is not the Heppner-Maynard distorted two-cell pattern, nor is it the simple four-cell pattern often drawn to support sun-

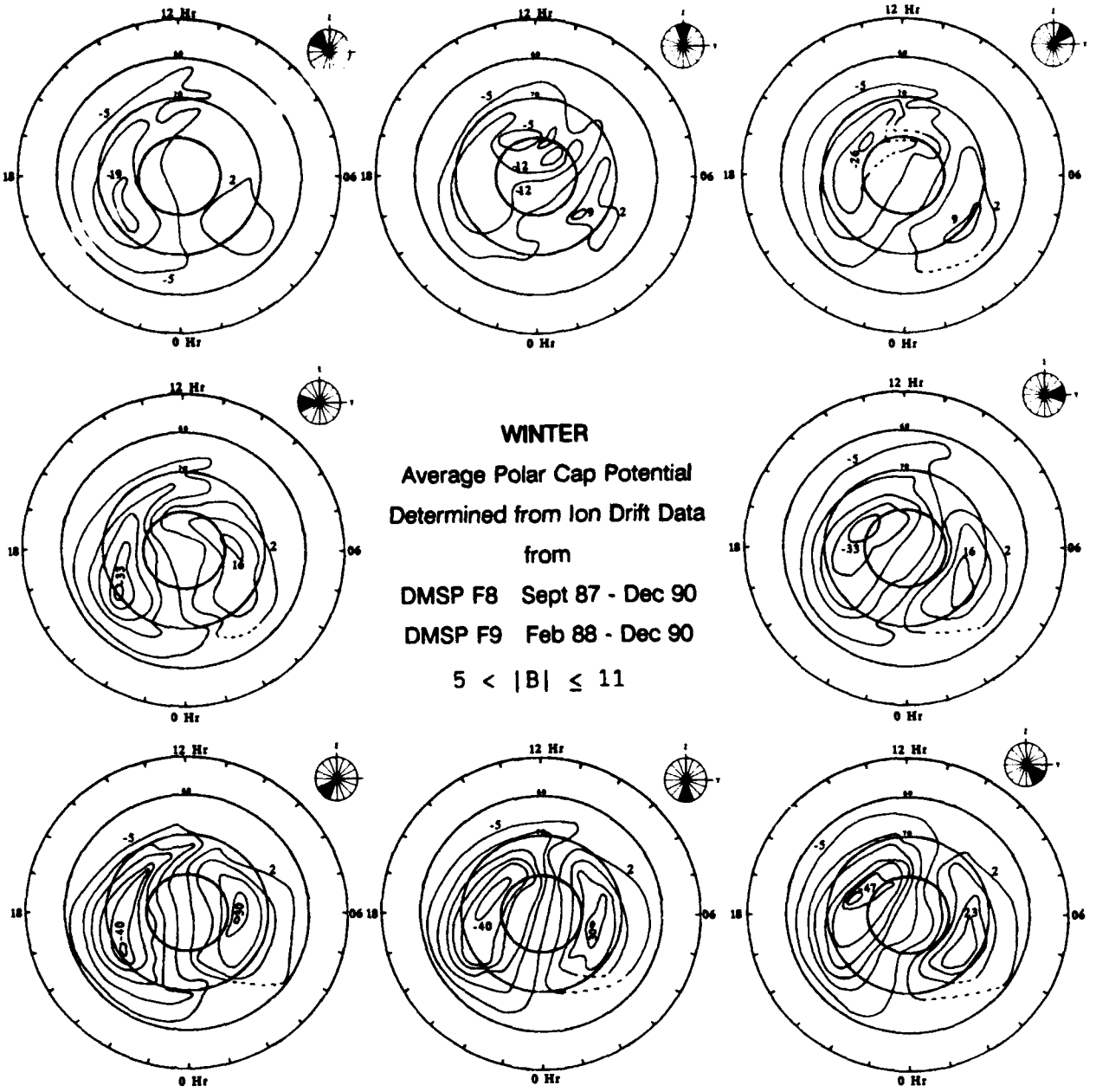

Figure 6. Contours drawn through the average potentials from DMSP F8 and F9 ion drift meter data obtained during winter solstice periods and for times when IMF data are available and 5 <| B |≤ 11 nT. The data are separated into 8 groups based on the IMF B_y/B_z angle. Format is identical to that of Figure 4. Winter solstice is defined to be May to July in the southern hemisphere and November to January in the northern hemisphere.

ward convection near the noon-midnight meridian in the polar cap.

2. The convection reversal boundary between the auroral zone and the polar cap is better described as a rotational discontinuity rather than as a shear boundary.

3. The average patterns do not show evidence for the Harang discontinuity near midnight as described in the Heppner-Maynard model.

Knowledge of the shape of the convection pattern is important both for understanding the ionosphere-magnetosphere connection, but also for studying the connection. Previous studies such as the one by *Reiff and Luhmann* [1986] have calculated the potential drop across the polar cap along a satellite track and have tried to pick tracks that were near the maximum and minimum in the potential pattern. With the use of this study and previous studies [e.g., *Heppner and Maynard*, 1987; *Foster et al.*, 1989], one should be able to adjust the observed cross-cap potential drop to a potential drop that is close to the drop between the global minimum and maximum potentials. In fact, *Lu et al.*

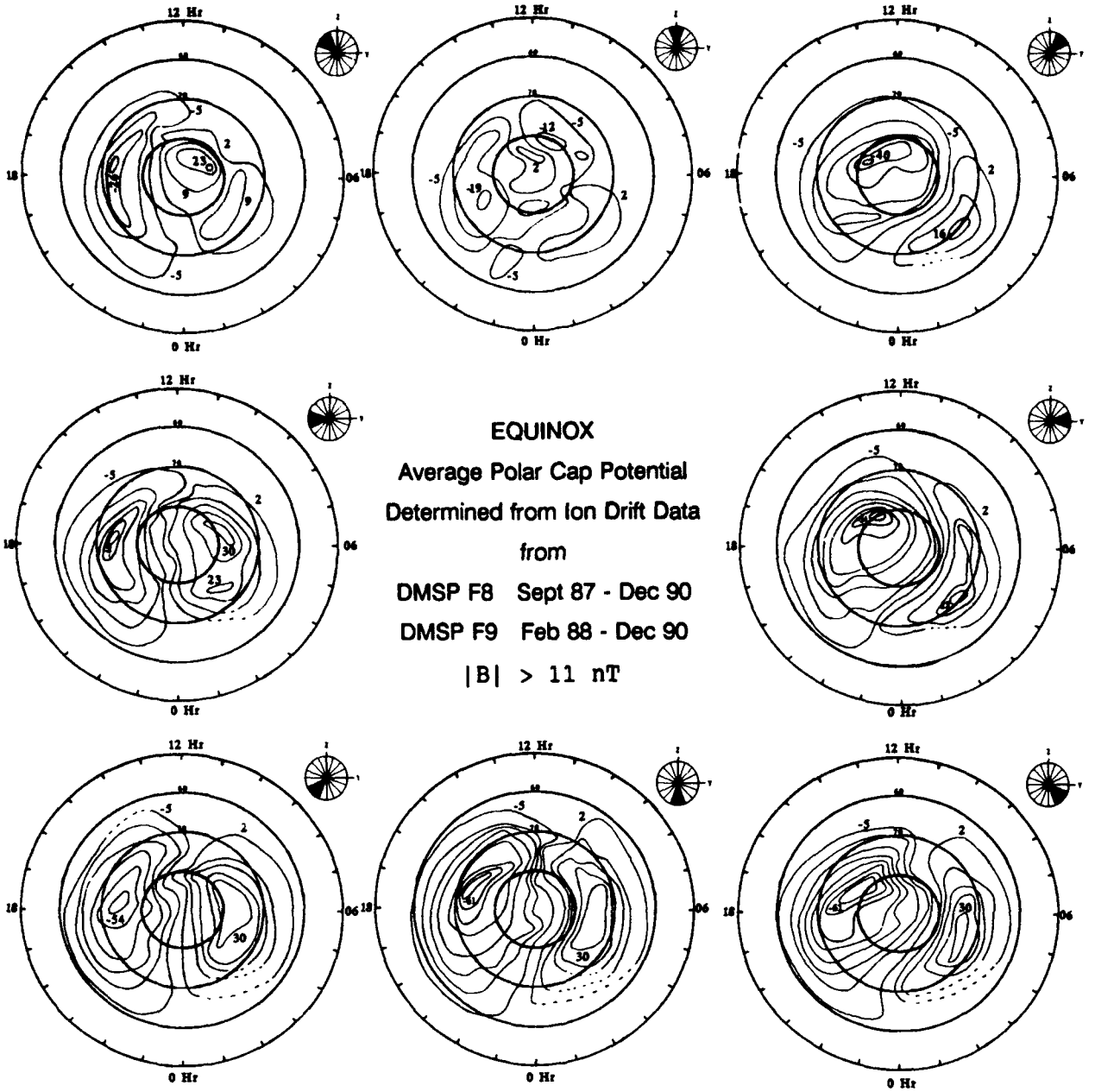

Figure 7. Contours drawn through the average potentials from DMSP F8 and F9 ion drift meter data obtained during equinox periods and for times when IMF data are available and $| B |> 11$ nT. The data are separated into eight groups based on the IMF B_y / B_z angle. Format is identical to that of Figure 4.

[1989] tried to find a "best" function for the variation of the max/min potential as a function of magnetic local time. Their results are similar to ours, but they could only match their data to a simple sine function due to the small data set available to them. If the study done by Reiff and Luhmann were redone using a function of potential versus magnetic local time, the conclusions might be the same, but the scatter in the data points to the proper functional description of the IMF-magnetosphere coupling should be significantly reduced. The advantages of using the result of this study compared to the previous studies is that we extend the range of conditions under which the potential pattern has been observed.

There are clearly limits to the usefulness of this or any other statistical study. There are many features that do not appear in the average pattern which may occur frequently in individual observations. For example, rapid ion flow ($\gg$1 km s^{-1}) is often observed near the dayside cusp, but average patterns do not show such strong convection. In this case and many other cases, the phenomenon is rapidly changing in magnitude and location. Any statistical analysis will spread the phenomenon over a large region where it is observed from

pass to pass and from day to day, and will decrease its magnitude. As a result, any statistical average is slightly invalid in describing in detail the state of the ionosphere at any given point in time. *Heppner and Maynard* [1987] tried to avoid this problem by showing "typical" patterns instead of a statistical pattern. Both methods have advantages, but both have disadvantages if taken too literally by the reader.

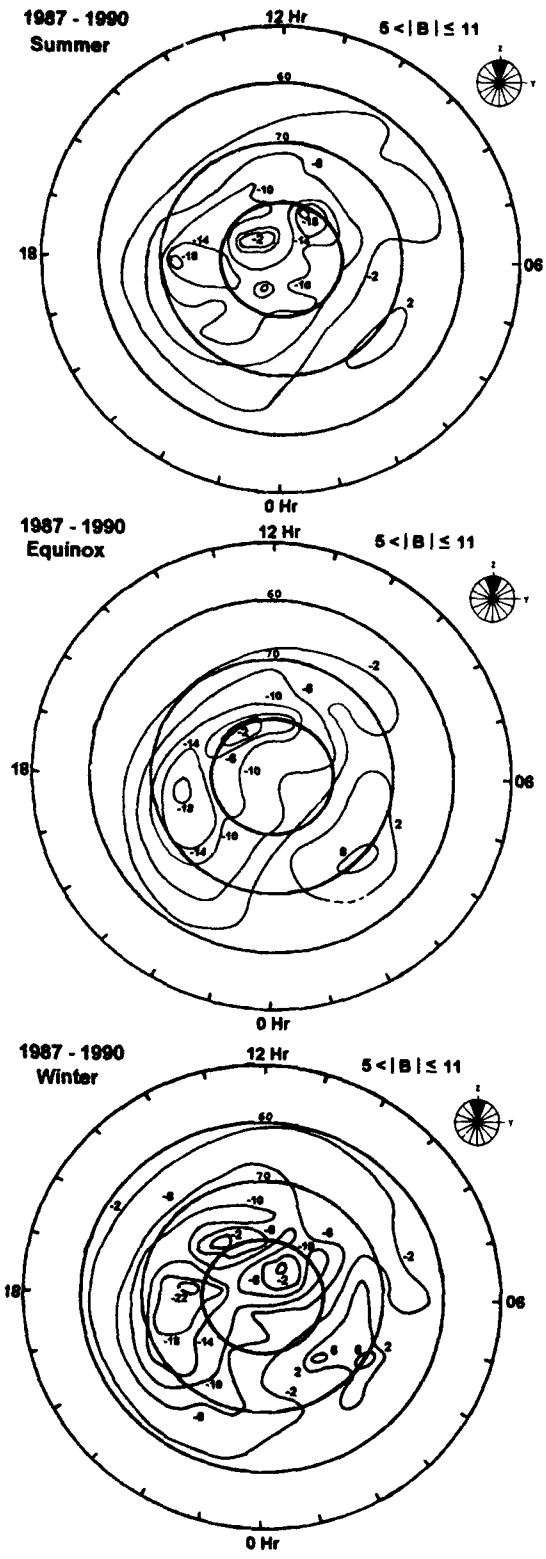

Figure 8. Contours from summer, equinox and winter for IMF $B_z > 0$ and $B_z > |B|_y|$. Each contour represents a change of 4 kV; all other characteristics are the same as Figure 4.

Arguments have been put forward that the convection reversal boundary should be a shear boundary, for all local time sectors except those near noon and midnight. If no plasma convects across the boundary then no potential contours will cross the boundary if the boundary is stationary. The concept is that the convection reversal boundary is at or near the open/closed field line boundary and thus maps to either the magnetopause or a region just inside the magnetopause for the dayside portion of the auroral oval and maps to the boundary between the boundary plasma sheet and the tail lobes in the midnight portion of the auroral oval. If potential contours cross the ionospheric boundary, then they should also cross the boundary at the distant end of the field line at the magnetopause or in the tail. This would imply significant connection between magnetosphere and the IMF. If connection occurs in a limited portion of the dayside magnetopause and reconnection occurs in a limited section of the plasma sheet–tail lobe boundary, then the potential contours cross the reversal boundary only in limited local time sectors near noon and midnight. This concept was the basis of the studies by *Moses et al.* [1988, 1989]. However, our results as well as the previous observational studies do not support this idea. There is a significant crossing of the convection reversal boundary by the potential contours in all local time sectors. Actually, the potential contours in Moses et al.'s dynamic model do cross the boundary without plasma flowing across the boundary because the boundary moves at the same speed as the plasma. In order to properly compare their results with ours, one needs to average the contracting oval potential contours with the expanding oval contours. The average of the Moses et al. potential contours would yield a broad shear boundary near the dusk and dawn meridians which is not evident in our results.

In our study, the IMF B_y/B_z angle has a much greater effect on the cross-polar cap potential drop and on the shape of the convection pattern than does either the magnitude of B or season. *Reiff and Luhmann* [1986] developed a relationship for the cross-cap potential as

$$\Phi(kV) = 6.7 + 0.047vB\sin^3(\theta/2) \qquad (5)$$

where v is the solar wind speed in kilometers per second; B is the IMF magnitude in nanoTesla and $B < 10$ nT; and θ is the IMF polar angle in GSM coordinates.

This formula suggests a stronger influence of the magnitude of the IMF than does this study. This is reconciled by noting that almost all of the observations used to derive (5) would fit into our single bin for $5 < B < 11$ nT. Also, we did not have access to solar wind plasma data. While the magnitude of B and v often correlate, sometimes they are anticorrelated. *Reiff and Luhmann* [1986] mention that Φ tends to go to a "saturation" value for large values of B.

Most previous studies of the potential have not shown a seasonal dependence to the potentials. This has been partially due to practical considerations and partially due to conceptual considerations. The practical consideration is that each group of investigators has used the type of data set available to them. For example, the studies based on ground-based magnetometer data of *Friis-Christensen et al.* [1985] and *Feldstein and Levitin* [1986] use only summer data since a high ionospheric conductivity is required to obtain data than can be easily analyzed. On the other hand, *Heppner and Maynard* [1987] had data from all seasons and noted a systematic variation of the potential drop between summer and winter. Because of their limited data set, they described the difference as not statistically significant. *Holt et al.* [1987] also separated their data for $Kp = 0$ to 4 by season and found minor differences which they did not believe to be statistically significant. Others, such as *Foster et al.* [1986a, b], have data from all seasons but fail to mention whether or not they observe a seasonal variation in the electric potential. Such a failure is understandable since there are theoretical arguments for the electric field being independent of season. The thought is that the electric potential is imposed as part of the process of merging of closed geomagnetic with the solar wind to create open field lines. When the field lines reconnect behind the Earth, they must be connected to both hemispheres. Assuming there are no significant and systematic field-aligned potential drops between the magnetopause and the ionosphere, the potential drop across both hemispheres should be the same. Our study suggests that there is a small but statistically significant difference in the potential drop and potential distribution between seasons. The study by *de la Beaujardiere et al.* [1991] is the only study we are aware of that shows a seasonal dependence for the potential pattern. Their dependence is similar, but not identical, to our results. *Crooker and Rich* [1993] suggest that some of the excess potential comes from merging of the open field lines in the lobes with the solar wind. The lobe is more accessible to the solar wind in the summer hemisphere than in the winter hemisphere.

Since *Burke et al.* [1979] pointed out that evidence for a multicell convection pattern existed during a period of northward directed IMF, there has developed a concept that all periods of northward directed IMF should exhibit similar behavior. In our study, for IMF $B_z > 0$, the two-cell convection pattern dominates the system. This is not due to a weak four-cell pattern being obscured by our averaging technique. An inspection of many passes during the equinox and summer seasons when IMF $B_z > 0$ showed no evidence for a four cell pattern. This does not imply that we never observed multicell convection in this data set. *Cumnock et al.* [1992] used this data set to study a period of several hours when IMF B_z was strongly northward and IMF B_y was changing. In that study a multicell pattern that seemed to evolve with the changing IMF direction was observed. *Knipp et al.* [1991] have presented evidence that a multicell pattern (or a distorted two-cell pattern with some of the same characteristics as a multicell pattern) develops over a period of time (> 40 min) with B_z being northward. On the other hand, there is evidence that when the IMF changes from northward to southward, the convection pattern responds faster than 40 min. We have not set up separated cases for times when the IMF has been northward for a short period of time and for times when it has been northward for a long period of time. Thus the persistence for tens of minutes of the southward pattern after the IMF has turned northward may have overwhelmed the northward pattern in our statistics.

For IMF $B_z > 0$ and $|B_y| \ll B_z$ (the top center pattern in Figures 4-7), a pattern emerges of two reverse convection cells within the afternoon cell of the normal two-cell pattern. This pattern is quite different from the four equally sized cells suggested by *Burke et al.* [1979] and is different from the two normal cells with a lobe cell or with the dominate reversed convection cells suggested by *Reiff and Burch* [1985]. On the other hand, our pattern bears some similarity to the pattern calculated by *Knipp et al.* [1991] during a period of northward IMF. In their pattern the two normal convection cells exist only in the nightside and the reverse convection cells exist only in the dayside.

When one looks at the ion drift data during winter passes when the IMF is northward, it seems difficult to obtain any pattern at all. At such times, the ion drift and the electric field inferred from it can be large (> 1 km s^{-1}) and rapidly changing in the spacecraft's frame of reference. Over short distances (a few hundred kilometers), the inferred electric field tends to integrate to very small potential drops in a pattern that is not repeatable from pass to pass. However, over larger scale sizes, we have found that there is a pattern which does tend to be repeatable. This is similar to the results obtained by *Bythrow et al.* [1985] with field-aligned current observations.

The average patterns do not show the strong Harang discontinuity in the local time sector 2200 to 2400 MLT presented by *Heppner and Maynard* [1987]. Instead our average contours in this sector are very similar to the results of *Foster et al.* [1986a, b] and *Holt el al.* [1987]. The Harang discontinuity is defined as the reversal of plasma flow from westward to eastward along a magnetic meridian in or near the auroral zone in the midnight sector. The Heppner-Maynard model indicates a Harang discontinuity with the convection reversal roughly in the middle of the auroral zone from 22 to 24 hours with eastward convection in the poleward portion of the auroral zone roughly as rapid as westward convection in the equatorward portion of the auroral zone. In addition, the Heppner-Maynard model shows no change in the Harang discontinuity as a function of IMF B_y and only a small change as a function of IMF B_z.

We have considered the possibility that the failure of our statistical convection model to match the Heppner-Maynard "typical" convection model in this respect is due to our statistical method. In our method, features which move or are formed from event to event in different locations with respect to our flexible magnetic coor-

dinates can be spread out so much that they do not seem to exist. When we inspect individual passes, we find that the strong Harang discontinuity of the Heppner-Maynard model is often, but not always missing from the 2200 to 2400 LT sector. To illustrate this point, the ion drift data for some representative passes through the auroral zone in the late evening sector are shown in Figure 9. In Figure 9a, the observed convection reversal approximately matches that expected from the Heppner-Maynard model. For the pass at 0120 UT, the convection reversal is at 65° geomagnetic latitude and 2310 MLT which is in the middle of the region of auroral electron precipitation. For the pass at 0304 UT, the satellite track is at earlier local times, and the reversal is located near the poleward edge of the auroral zone. This pattern does not appear in the statistical model because it is outweighed by many other passes which do not share this pattern. In Figure 9b, a pattern of convection which is more representative of the DMSP data set is shown. On March 4, 1989, the convection reversal was observed near the poleward boundary of the auroral zone on the passes through the 2300 MLT sector as well as the pass through the 2200 MLT sector. The rapid eastward convection on poleward boundary of the auroral zone is a very common feature of the DMSP data, but even this is not clearly observed in the statistical model. First, the rapid eastward convection on the poleward boundary is not always observed, and second, the poleward boundary is variable with respect to the equatorward boundary, which was used to normalize the model's coordinate system.

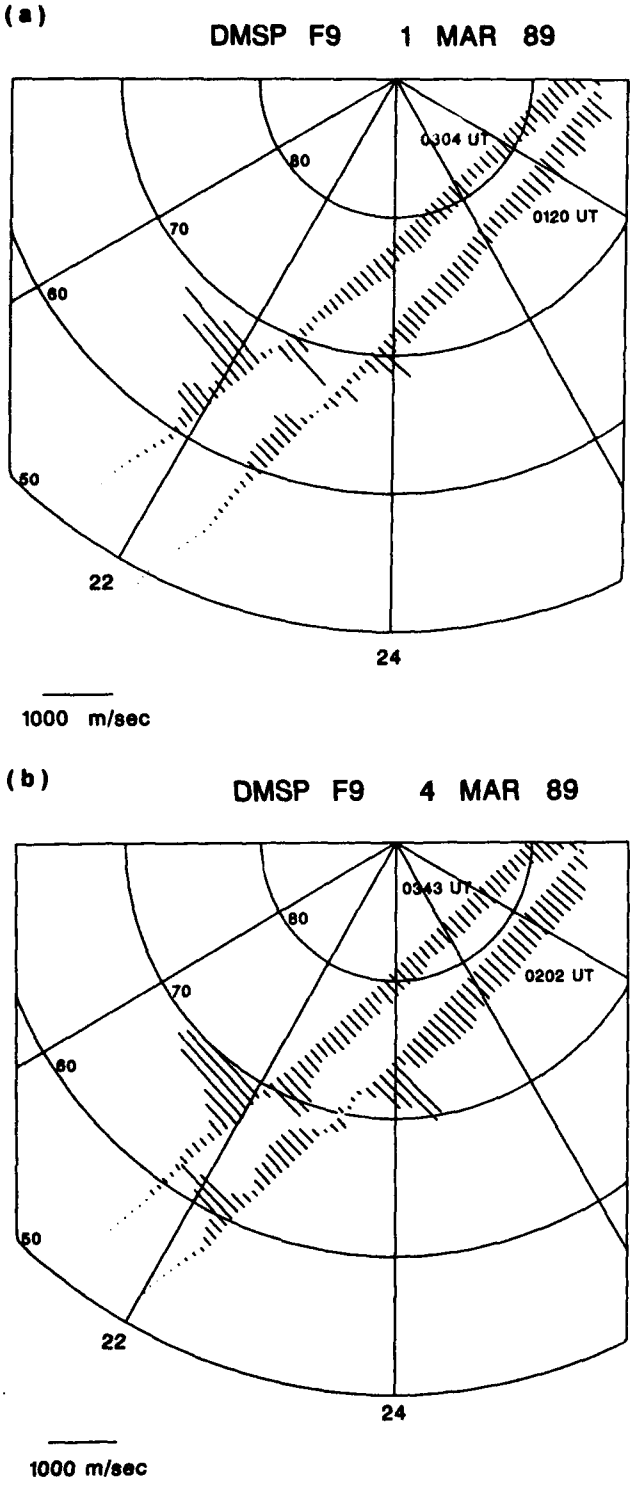

Figure 9. Ion drift plots (cross-track component only) in magnetic local time and geomagnetic latitude coordinates. Shaded lines along satellite path indicate region of auroral electron precipitation. (a) Two passes of F9 through the premidnight sector in the northern hemisphere on March 1,1989 when $Kp = 4-$, (b) Two passes of F9 through the premidnight sector in the northern hemisphere on March 4, 1989 when $Kp = 3+$.

While our results in the Harang discontinuity are distinctly different from the Heppner-Maynard model, they do not represent fundamentally different observations. The observations for individual passes which were presented by *Maynard* [1974] and which helped to shape the thinking behind the Heppner-Maynard model are very similar to the observations obtained with the ion drift meter on the DMSP F9 satellite. The Harang discontinuity, like the dayside cusp, is a very dynamic feature that does not lend itself well to being described statistically. The Harang discontinuity is often more pronounced in individual observations than in the statistical model. On the other hand, the sharply bent contours of potential representing the Harang discontinuity in the Heppner-Maynard model are too sharply bent and/or too far from the poleward boundary of the auroral zone to represent many individual observations.

Acknowledgments. The interplanetary magnetic field data from IMP 8 was provided by Ron Lepping of NASA/GFSC and by the National Space Science Data Center. We thank W. F. Denig for the assistance with the IMF data. This work was supported in part by task 2311G5 of the Air Force Office of Scientific Research and under contract F19628-90-K-0002 between PL/GP and UTD.

The Editor thanks J. C. Foster and an other referee for their assistance in evaluating this paper.

References

Ahn, B.-H., Y. Kamide, H. W. Kroehl and D. J. Gorney, Cross-polar cap potential difference, auroral electrojet indices and solar wind parameters, *J. Geophys. Res., 97,* (A2), 1345-1352, 1992.

Axford, W. I., and C. O. Hines, A unifying theory of high-latitude geophysical phenomena, *Can. J. Phys., 39,* 1433, 1961.

Burch, J. L., C. Gurgiolo, and J. D. Menietti, The electron signature of parallel electric fields, *Geophys. Res. Lett., 17,* (12), 2329-2332, 1990.

Burke, W. J., M. C. Kelley, R. C. Sagalyn, M. Smiddy, and S. T. Lai, Polar cap electric field structures with a northward interplanetary magnetic field, *Geophys. Res. Lett., 6,* (1), 21-24, 1979.

Bythrow, P. F., W. J. Burke, and T. A. Potemra, Ionospheric evidence for irregular reconnection and turbulent plasma flow in the magnetotail during periods of northward interplanetary magnetic field, *J. Geophys. Res., 90,* (A6), 5319-5325, 1985.

Cumnock, J. A., R. A. Heelis and M. R. Hairston, The response of the ionospheric convection pattern to a rotation of the IMF on January 14, 1988, *J. Geophys. Res., 97,* (A12), 19,449-19,460, 1992.

Crooker, N. U. and F. J. Rich, Lobe-cell convection as a summer phenomenon, *J. Geophys. Res., 98,* (A8), 13,403-13,407, 1993.

de la Beaujardiere, O., D. Alcayde, J. Fontanari, and C. Leger, Seasonal dependence of high-latitude electric fields, *J. Geophys. Res., 96,* (A4), 5723-5735, 1991.

Feldstein, Y. I., and A. E. Levitin, Solar wind control of electric fields and currents in the ionosphere, *J. Geomagn. Geoelectr., 38,* 1143-1182, 1986.

Foster, J. C., J. M. Holt, and R. G. Musgrove, Ionosphere convection associated with discrete levels of particle precipitation, *Geophys. Res. Lett., 13,* (7), 656-659, 1986a.

Foster, J. C., J. M. Holt, R. G. Musgrove, and D. S. Evans, Solar wind dependencies of high-latitude convection and precipitation, 477 - 494, *Solar Wind-Magnetosphere Coupling,* edited by Y. Kamide and J. Slavin, Terra Scientific, Tokyo, 1986b.

Foster, J. C., T. Fuller-Rowell, and D. S. Evans, Quantitative patterns of large-scale field-aligned currents in the auroral ionosphere, *J. Geophys. Res., 94,* (A3), 2555-2564, 1989.

Friis-Christensen, E., Y. Kamide, A. D. Richmond, and S. Matsushita, Interplanetary magnetic field control of high-latitude electric fields and currents determined from Greenland magnetometer data, *J. Geophys. Res., 90,* (A2), *1325-1338, 1985.*

Greenspan, M. E., P. B. Anderson, and J. M. Pelagatti, Characteristics of the thermal plasma monitor (SSIES) for the Defense Meteorological Satellite Program (DMSP) spacecraft S8 through F10, Tech. Rep. *AFGL-TR-86-0227,* Hanscom AFB, Mass., 1986.

Gussenhoven, M. S., D. A. Hardy, and N. Heinemann, Systematics of the equatorward diffuse auroral boundary, *J. Geophys. Res., 88,* (A7), 5692-5708, 1983.

Heelis, R. A., W. B. Hanson, and J. L. Burch, Ion convection reversals in the dayside cleft, *J. Geophys. Res., 81,* (22), *3803-3810, 1976.*

Heelis, R. A., W. B. Hanson, C. R. Lippincott, D. R. Zuccarro, L. H. Harmon, B. J. Holt, J. E. Doherty, and R. A. Power, The ion drift meter for Dynamics Explorer B, *Space Sci. Instrum., 5,* (4), 511-522, 1981.

Heppner, J. P., Polar cap electric field distributions related to the interplanetary magnetic field directions, *J. Geophys. Res., 77,* (25), 4877, 1972.

Heppner, J. P., and N. C. Maynard, Empirical high-latitude electric field models, *J. Geophys. Res., 92,* (A5), 4467-4489, 1987.

Holt, J. M., R. H. Wand, J. V. Evans, and W. L. Oliver, Emperical models for plasma convection at high latitudes from Millstone Hill observations, *J. Geophys. Res., 92,* (A1), 203-212, 1987.

Kamide, Y., B. H. Ahn, S. I Akasofu, W. Baumjohann, E. Friis-Christensen, H. W. Kroehl, H. Maurer, A. D. Richmond, G. Rostoker, R. W. Spiro, J. K. Walker, and A. N. Zaitzev, Global distribution of ionospheric and field-aligned currents during substroms as determined from six IMS meridian chains of magnetometers: Initial results, *J. Geophys. Res., 87,* (A10), 8228-8240, 1982.

Knipp, D. J., A. D. Richmond, B. Emery, N. U. Crooker, O. de la Beaujardiere, D. Evans, and H. Kroehl, Ionospheric convection response to changing IMF direction, *Geophys. Res. Lett., 18,* (4), 721-724, 1991.

Lockwood, M., Flux transfer events at the dayside magnetopause: Transient reconnection or magnetosheath dynamic pressure pulses?, *J. Geophys. Res., 96,* (A4), 5497-5509, 1991.

Lockwood, M., and S. W. H. Cowley, Comment on "ionospheric convection response to changing IMF direction" by Knipp et al., *Geophys. Res. Lett., 18,* (11), 2173-2174, 1991.

Lockwood, M., S. W. H. Cowley, and M. P. Freeman, The excitation of plasma convection in the high-latitude ionosphere, *J. Geophys. Res., 95,* (A6), 7961-7972, 1990.

Lu, G., P. H. Reiff, M. R. Hairston, R. A. Heelis, and J. L. Karty, Distribution of convection potential around the polar cap boundary as a function of the interplanetary magnetic field, *J. Geophys. Res., 94,* (A10), 13447-13461, 1989.

Lu, G., A. D. Richmond, B. A. Emery, P. H. Reiff, O. de la Beaujardiere, F. J. Rich, W. F. Denig, H. W. Kroehl, L. R. Lyons, J. M. Ruohoniemi, P. T. Newell, D. S. Evans, E. Friis-Christensen, H. Opgenoorth, J. Foster, R. P. Lepping, A. S. Rodger, T. Hughes, H. Nevanlinna, C. G. Macleannan, A. McEwin, S. Dennis, R. Morris, G. Burns, and L. Tomlinson, Interhemispheric asymmetry of the high-latitude ionosphere convection pattern, *J. Geophys. Res.*, in press, 1993.

Madden, D., and M. S. Gussenhoven, Auroral boundary index from 1983 to 1990, Tech. Rep. *GL-TR-90-0358,* Hanscom AFB, Mass., 1990.

Maynard, N., Electric field measurements across the Harang discontinuity, *J. Geophys. Res., 79,* (31), 4620-4631, 1974.

Moses, J. J., G. L. Siscoe, R. A. Heelis, and J. D. Winningham, A model for multiple throat structures in the polar cap flow entry region, *J. Geophys. Res., 93,* (A9), 9785-9790, 1988.

Moses, J. J., G. L. Siscoe, R. A. Heelis, and J. D. Winningham, Polar cap deflation during magnetospheric substorms, *J. Geophys. Res., 94,* (A4), 3785-3789, 1989.

Reiff, P. H., and J. L. Burch, IMF B_y dependent plasma flow and Birkeland currents in the dayside magnetosphere, 2. A global model for northward and southward IMF, *J. Geophys. Res., 90,* (A2), 1595-1609, 1985.

Reiff, P. H., and J. G. Luhmann, Solar wind control of the polar cap potential, 453 - 476, *Solar Wind-Magnetosphere Coupling,* edited by Y. Kamide and J. Slavin, Terra Scientific, Tokyo, 1986.

Reiff, P. H., H. L. Collin, J. D. Craven, J. L. Burch, J. D. Winningham, E. G. Shelley, L. A. Frank and M. A. Friedman, Determination of auroral electrostatic potentials using high- and low-altitude particle distributions, *J. Geophys. Res., 93,* (A7), 7441-7465, 1988.

Rostoker, G., D. Savoie and T. D. Phan, Response of magnetosphere- ionosphere current systems to changes in the interplanetary magnetic field, *J. Geophys. Res., 93,* (A7), 8633-8641, 1988.

Toffeletto, F. R., and T. W. Hill, Mapping of the solar wind electric field to the Earth's polar caps, *J. Geophys. Res., 94,* (A1), 329-347, 1989.

Wand, R. H., and J. V. Evans, The penetration of convection

electric fields to the latitude of Millstone Hill ($\Lambda = 56°$), *J. Geophys. Res., 86,* (A7), 5809-5814, 1981.

Weimer, D. R., C. K. Goertz, D. A. Gurnett, N, C. Maynard, and J. L. Burch, Auroral zone electric field from DE-1 and DE-2 at magnetic conjunctions, *J. Geophys. Res., 90,* (A8), 7479-7492, 1985.

Zuccaro, D., and B. J. Holt, A technique for establishing a reference potential on satellites in planetary ionospheres, *J. Geophys. Res., 87,* (A10), 8327-8329, 1982.

Marc Hairston, Center for Space Science, F022, P.O. Box 830688, University of Texas at Dallas, Richardson, Texas 75083-0688. (e-mail: hairston@utdssa.utdallas.edu)

Frederick J. Rich, Phillips Lab., Geophysics Dir., PL/GPS, Hanscom AFB, Massachusetts 01731-3010. (email: rich@plh.af.mil)

(Received January 13, 1993; revised August 25, 1993; accepted November 9, 1993.)